Fiber-Optic Links Supporting Baseband Data and Subcarrier-Multiplexed Control Channels and the Impact of MMIC Photonic/Microwave Interfaces

Daniel J. Blumenthal, *Member, IEEE,* Joy Laskar, *Member, IEEE,* Roberto Gaudino, Sangwoo Han, *Member, IEEE,* Michael D. Shell, and Mark D. Vaughn

***Abstract*— We report experimental and analytical results of a fiber-optic link that supports simultaneous transmission of baseband data and subcarrier multiplexed control-data channels. A novel transmitter design is used to optoelectronically combine baseband and subcarrier channels onto the optical carrier using a differential Mach–Zehnder (MZ) interferometer modulator. Microwave direct detection of the subcarrier data channel simplifies the receiver design and network architecture. An approach to optimize the transmitter parameters for a given transmitter/receiver configuration is presented. A discrete component link is implemented and its performance compared to analytical results and discrete-time simulations. Insertion of monolithic-microwave integrated-circuit (MMIC) technology is investigated by utilizing a MMIC mixer for control-channel upconversion and envelope detection in the link transmitter and receiver, respectively. High signal-to-noise ratio (SNR) of the control channel demonstrates that MMIC technology is a viable approach to integration of subcarrier multiplexed fiber links.**

***Index Terms*— Communication system signaling, microwave devices, microwave modulation/demodulation, MMIC receivers/transmitters, optical communications, optical modulation, optical subcarrier multiplexing.**

I. Introduction

FIBER-OPTIC networks offer the potential to support very wide-band flexible communications for future analog and digital applications. The large available bandwidth of a fiber network can support multichannel communications using wavelength division multiplexing (WDM), optical subcarrier multiplexing (OSCM) [1], [2], and combination WDM–OSCM techniques [3], [4]. A primary advantage of multichannel transmission in the fiber is that the network interface electronics can be operated at the individual channel rate. The different channels (wavelength, frequency, or optical subcarrier) can be used to support independent users or to transmit out-of-band signals, e.g., routing or timing information. The latter has received increasing attention in fiber networks since information can be transmitted and recovered in parallel without a fixed clock or timing relationship between the data and control channels. Detection of subcarrier coded channels is performed using simple photodetection followed by microwave bandpass filtering.

In this paper, we describe results of our work in OSCM links for transmitting digital baseband data in parallel with a subcarrier multiplexed control-data channel and the potential for monolithic-microwave integrated-circuit (MMIC) technology at the photonic/microwave interfaces. Baseband/OSCM-control fiber links can support various functions for different network architectures including the setup of end-to-end connections in a circuit-switched network [5], [6], contention resolution in circuit- and packet-switched networks [7], and to support header transmission in packet-based networks [8]–[11].

Important issues for these links currently include component and subsystem integration and performance limitations due to fiber dispersion and nonlinearities [12]. The integration aspects involve fabrication of basic circuits for microwave signal generation, upconversion of digital data streams, and combining baseband and subcarrier multiplexed signals onto an optical carrier. New techniques are needed to efficiently interface microwave and photonic components at the transmitter and receiver [13], [14]. Circuit complexity and link performance are related through the choice of subcarrier data-modulation format, incoherent or coherent detection, the integration technology, and the overall systems architecture. These techniques should ultimately support digital baseband rates beyond 40 Gbps and subcarrier signals beyond 50 GHz.

In this paper, we report new experimental and theoretical results of a digital baseband/OSCM-control transmission link for optical and all-optical-fiber networks. A novel transmitter architecture based on a differentially driven integrated-optic Mach–Zehnder (MZ) interferometer enables optoelectronic combining of baseband data with microwave subcarrier modulated control data. A microwave direct-detection receiver for the subcarrier data channel is employed to simplify the receiver design and network architecture. The optoelectronic baseband/SCM combining approach simplifies the transmitter design and reduces losses as compared to electronic combining techniques [10]. A MMIC-based mixer element is designed, fabricated, and inserted into the transmitter and receiver for

Manuscript received December 5, 1996; revised April 28, 1997. The work of D. J. Blumenthal was supported by the NSF Young Investigator Award ECS-9457148 and by the DARPA DURIP Award DAAH04-96-1-0346. The work of J. Laskar was supported by the NSF Career Award ECS-9623964 and the ARO Young Investigator Award DAAH04-95-1-0397. The work of R. Gaudino was supported by the Associazione Elettrotecnica Italiana (AEI) scholarship ECOC'95.

D. J. Blumenthal, J. Laskar, S. Han, M. Shell, and M. D. Vaughn are with the Microelectronics Research Center, School of Electrical and Computer Engineering, Georgia Institute of Technology, Atlanta, GA 30332-0250 USA.

R. Gaudino is with the Dipartimento di Elettronica, Politecnico di Torino, Torino, Italy.

Publisher Item Identifier S 0018-9480(97)06005-5.

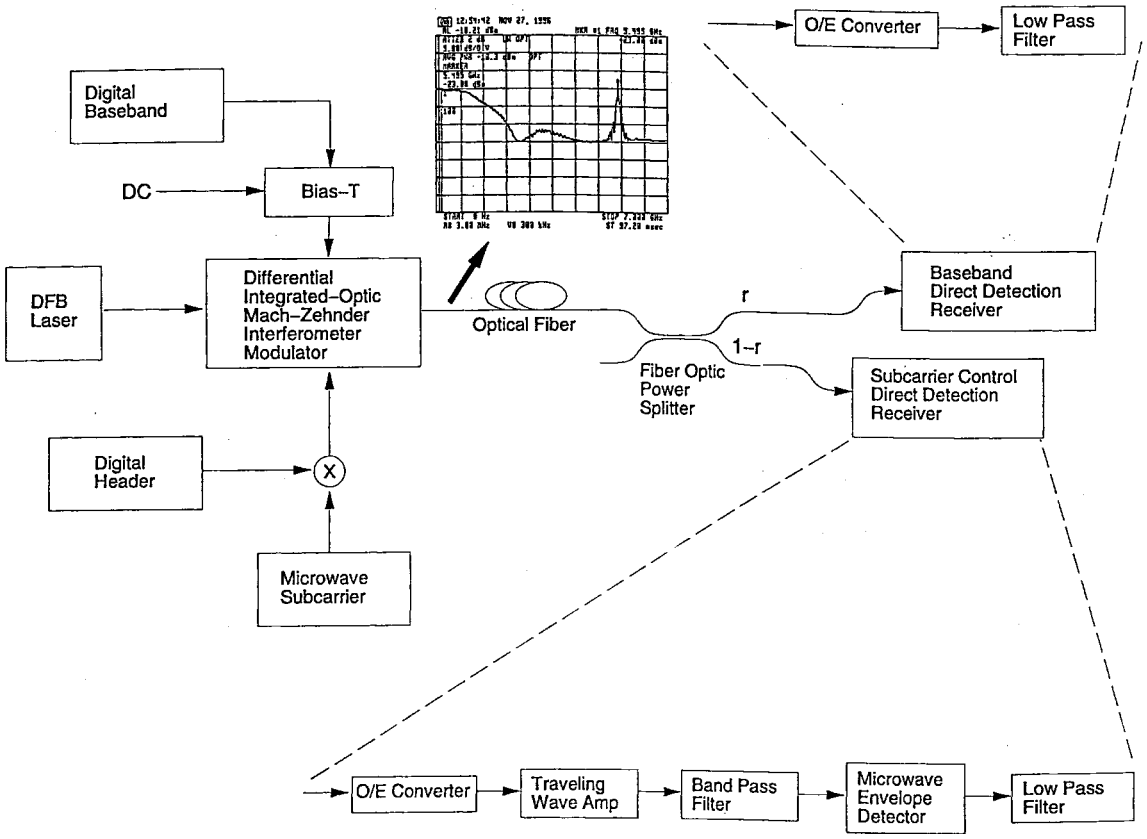

Fig. 1. General architecture of baseband/OSCM link with differential MZ interferometer modulator together with the power spectrum of composite 2.5-Gbps PRBS baseband with 100-Mbps PRBS control on 5.5-GHz subcarrier.

upconversion and envelope detection, respectively. The received signal-to-noise ratio (SNR) is comparable to results obtained with discrete component implementation and demonstrates that MMIC technology offers a viable approach to photonic/microwave interface integration for this type of link. Analysis of the differential nonlinear transmitter is presented and includes optimization of the relative SNR for the received baseband/OSCM channels. This analysis extends the results of prior work in optimum modulation for baseband/OSCM transmission by direct linear modulation of a semiconductor laser [9].

II. Link Architecture

The fiber-optic link investigated in this paper is capable of supporting simultaneous transmission of baseband digital data and microwave subcarrier multiplexed digital control data on a single optical carrier. The general link architecture is shown in Fig. 1 with a digital baseband/subcarrier transmitter, optical-fiber transmission channel and baseband and subcarrier control receivers. The baseband and control-data receivers are located after a variable optical-power splitter. The introduction of a variable splitter accommodates multiple network architectures including header detection receivers for packet routing [8], [15]–[17] and end-node detection for connection-oriented transmission [18].

The transmitter consists of two data sources, one for digital baseband and the other for the digital control channel. A novel optoelectronic technique is used to combine the baseband data with the microwave-subcarrier control data [15], reducing the transmitter complexity and alleviating the need for an electronic summing circuit which introduces excess resistive loss. One arm of a differential-input integrated-optic MZ interferometer modulator is driven by dc-biased baseband data and the other arm is driven by the microwave subcarrier control data. Differential driving of the two arms acts to combine the baseband and subcarrier multiplexed signal onto the optical output of a continuous wave, distributed feedback (DFB) semiconductor laser. Differential MZ interferometer modulators are typically used to minimize optical chirp at very high data modulation rates. An example experimental composite baseband/OSCM electronic-power spectrum is shown in Fig. 1 with actual data rates and subcarrier frequency used in the experimental section of this paper (2.5-Gb/s baseband data rate and 100-Mb/s control-channel data rate multiplexed onto a 5.5-GHz subcarrier).

The baseband and control-channel receivers each detect a portion of the optical power determined by the network architecture requirements. A fiber splitter is used to tap a portion of the optical signal for the subcarrier receiver and output the remaining signal to the baseband receiver. The baseband receiver consists of a simple optical-to-electrical (O/E) converter and a low-pass filter to pass the digital baseband and reject the subcarrier channel. The subcarrier direct-detection receiver consists of an O/E converter followed by a broad-band traveling-wave amplifier, a bandpass filter centered at the subcarrier frequency to reject the baseband data, a microwave envelope detector, and finally, a low-pass filter.

III. Link Design and Optimization

In this section, we develop an analytical model which allows the optimization of the input transmitting parameters given a certain link and receiver configuration taking into account the nonlinear transfer function of the modulator. The signal applied to the electrical port of the modulator can be written as

$$V(t) = V_d(a\alpha(t) + b\beta(t)\cos(2\pi f_s t + \phi) + c) \qquad (1)$$

where V_d is an arbitrary voltage, $\alpha(t) = 0,1$ is the baseband data at bit-rate $B_{\text{base}} = 1/T_{\text{base}}$, $\beta(t) = 0,1$ is the control-channel data at bit-rate $B_{\text{cont}} = 1/T_{\text{cont}}$, f_s is the subcarrier frequency, ϕ is a constant phase, aV_d is the baseband input amplitude, bV_d is the control-channel input amplitude, and cV_d is the bias voltage.

We assume on–off keying (OOK) modulation on both baseband and subcarrier control channels. Other modulation techniques (PSK, FSK) for the control channel can be easily taken into account by choosing different values for β and letting ϕ change at the control-channel bit-rate. We also assume that the electrical bandwidth of the modulator is greater than the subcarrier frequency f_s, so that the transfer function of the modulating device can be expressed as an instantaneous nonlinear relation of the form

$$\begin{aligned} P(t) &= P_{\text{out}} f(V(t)) \\ &= P_{\text{out}} f(V_d(a\alpha(t) + b\beta(t)\cos(2\pi f_s t + \phi) + c)) \end{aligned} \qquad (2)$$

where P_{out} is the maximum output power, provided that $f(V)$ is normalized such that its maximum value with respect to V is equal to 1.

The relationship between the modulator transfer function and the baseband and OSCM control signal is illustrated in Fig. 2. The baseband data sets large signal quiescent operating points about which the relatively smaller subcarrier signal modulates. In order to increase baseband performance, the on/off operating points should be separated as far as possible placing the quiescent points at the max and min of the modulator transfer function. However, these operating points produce maximum nonlinear distortion of the subcarrier channel, reducing the overall SNR and increasing interference between the baseband and subcarrier channel due to intermodulation distortion. An optimum operating condition will specify the point at which both the baseband excursion and RF-signal strength can be maximized without producing a severe SNR degradation of either channel. From another, more physical, point of view, the small signal gain seen by the subcarrier signal reduces when increasing the baseband signal amplitude.

To analyze the effects of a nonlinear transfer function we expand (3) in a Taylor series around $b \to 0$, obtaining

$$\begin{aligned} \frac{P(t)}{P_{\text{out}}} \simeq\ & f(a\alpha(t)+c) + f_1(a\alpha(t)+c)b\beta(t)\cos(2\pi f_s t + \phi) \\ & + \frac{1}{2} f_2(a\alpha(t)+c)b^2\beta^2(t)\cos^2(2\pi f_s t + \phi) \\ & + \frac{1}{6} f_3(a\alpha(t)+c)b^3\beta^3(t)\cos^3(2\pi f_s t + \phi) \end{aligned} \qquad (3)$$

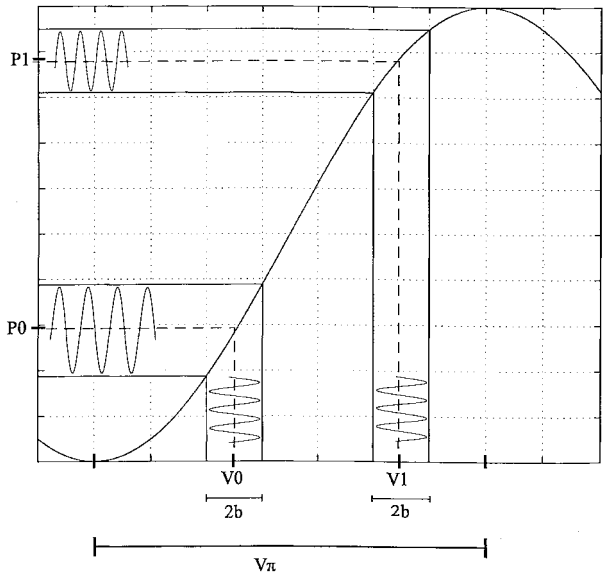

Fig. 2. Representation of baseband- and subcarrier-signal operating points on the MZ transfer function.

where the functions f_i are the i-order derivative of the function f. We have verified, through time-domain simulations, that the error introduced by truncating the Taylor series to the third-order term is negligible in all cases of practical interest.

For this transmission system we are interested in those terms whose spectral components can pass through the two receiving filters, i.e., in terms around $f = f_s$ for the control signal and $f = 0$ for the baseband signal. Using the relations $\beta^2(t) = \beta^3(t) = \beta(t)$ and the expansions for $\cos^2(x)$ and $\cos^3(x)$ we can rewrite (3) as

$$\begin{aligned} \frac{P(t)}{P_{\text{out}}} \simeq\ & f(a\alpha(t)+c) + f_1(a\alpha(t)+c)b\beta(t)\cos(2\pi f_s t + \phi) \\ & + \frac{1}{4} f_2(a\alpha(t)+c)b^2\beta(t) \\ & + \frac{1}{8} f_3(a\alpha(t)+c)b^3\beta(t)\cos(2\pi f_s t + \phi). \end{aligned} \qquad (4)$$

The first two terms can be interpreted as the useful baseband and control-data output components. The last two terms account for nonlinear beating between baseband and control data around $f = 0$ and $f = f_s$. Several important conclusions can be drawn from (4). The useful baseband term $f(a\alpha(t) + c)$ is dependent on the bias c and on the baseband input amplitude a only. The useful control-channel term $f_1(a\alpha(t) + c)b\beta(t)\cos(2\pi f_s t + \phi)$ does not depend on b only, but on a and c as well and is consequently affected by the values chosen for the baseband. Moreover, the output control-data instantaneous power is modulated by the baseband data, giving rise to interchannel interference between baseband and control signals. This interference can be minimized if

$$f_1(a + c) = f_1(c). \qquad (5)$$

We show in a following section, that in the case of MZ modulators, for any a, the optimal c is always the one satisfying (5), and corresponds to a situation where the two

baseband operating points are symmetric with respect to the middle point of the transfer function.

Introducing the baseband operating points $V_1 = V_d(a+c)$ and $V_0 = V_d\,c$ corresponding to the transmission of a 1 or a 0 bit, the output useful baseband levels can be expressed as $P_1 = P_{\text{out}} f(V_1)$, $P_0 = P_{\text{out}} f(V_0)$. The control data has an instantaneous power oscillating around P_1 or P_0 with a peak-to peak swing varying between $P_{\text{out}} f_1(V_1)\,b$ and $P_{\text{out}} f_1(V_0)\,b$ at the payload rate. A graphical representation of this condition is illustrated in Fig. 2. Restricting attention to a MZ external modulator, we have

$$P(t) = P_{\text{out}} f(V) = P_{\text{out}} \cos^2\left(\frac{\pi}{2}\frac{V}{V_\pi}\right) \tag{6}$$

with V_π is the switching voltage of the modulator and P_{out} is the output power when $V = 0$. We assume that $V_d = V_\pi$ so that, substituting (1) in (6), we obtain

$$P(t) = P_{\text{out}} \cos^2\Big(\frac{\pi}{2}(a\alpha(t) + b\beta(t)\cos(2\pi f_s t + \phi) + c)\Big) \tag{7}$$

where a and b represent the input amplitudes, normalized to V_π, for the baseband and control data, respectively. We restrict our attention to the case in which the driving voltage is in the range $[-V_\pi, 0]$ (any other choice $[(n-1)V_\pi, n\,V_\pi]$ would lead to identical results). If no control data is present, the optimal choice is ideally $V_0 = -V_\pi$ and $V_1 = 0$ (corresponding to a =1, $c = -1$) which gives $P_1 = P_{\text{out}}$ and $P_0 = 0$, i.e., an infinite extinction ratio. Under these circumstances, $f_1(V_0) = f_1(V_1) = 0$.

For control data alone, the optimum point is clearly the one that maximizes f_1, i.e., $V_0 = V_1 = -V_\pi/2$. Consequently, when both baseband and subcarrier are applied, a tradeoff exists between the two extreme situations in terms of system performances. In [9], analytical formulas are obtained for the digital SNR Q on both baseband and subcarrier for several different receiver configurations. Here, the Q parameter is defined as $Q = \frac{m_1 - m_0}{\sigma_1 + \sigma_0}$, where m_1 (m_0) is the average of the detected signal at the receiver when a 1, (0) is transmitted and σ_1^2, (σ_0^2) the corresponding variance. The probability of bit-error (BE) can be approximated as $P_e \simeq 1/2\,\text{erfc}(\text{Q}/\sqrt{2})$. A value $Q = 6$ corresponds to $P_e \simeq 10^{-9}$. Initially, we chose the simplified model whose performances are limited by electrical receiver noise. Let r be the splitting ratio of the optical coupler, ρ_{base}, ρ_{cont} the responsivities of the photodiodes, and N_{base}, N_{cont} the power-spectral densities of the equivalent noise sources. The filters and the envelope detectors are assumed to be ideal (integrate and dump filters) to obtain an analytical expression. Following the steps outlined in [9], the Q values of this receiver can be written as

$$Q_{\text{base}} = \frac{r\rho_{\text{base}} P_{rx} A_{\text{base}}}{\sqrt{2N_{\text{base}} B_{\text{base}}}}$$
$$Q_{\text{cont}} = \frac{(1-r)\rho_{\text{cont}} P_{rx} A_{\text{cont}}}{\sqrt{2N_{\text{cont}} B_{\text{cont}}}} \tag{8}$$

where $P_{rx} = P_{\text{out}} L$ and L is the total link loss and A_{base} is the normalized output baseband swing ($A_{\text{base}} = f_0(a+c) - f_0(c)$ when $b = 0$) and A_{cont} is the average normalized output control-data amplitude.

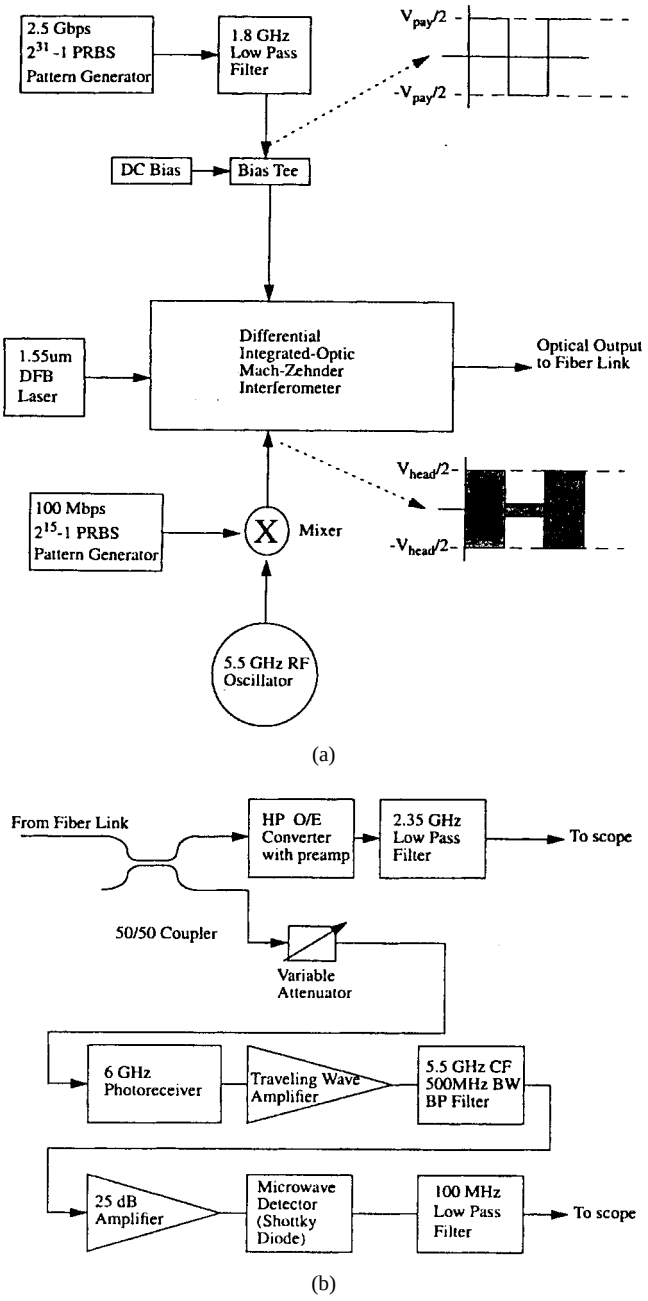

Fig. 3. Experimental setup for (a) differential baseband/OSCM transmitter and (b) receiver.

Using (4), the parameters A_{base} and A_{cont} can be expressed as

$$A_{\text{base}} = f_0(a+c) - f_0(c) + \frac{b^2}{4}(f_2(a+c) - f_2(c))$$
$$A_{\text{cont}} = \frac{1}{2}(f_1(a+c) + f_1(c)) + \frac{b^3}{16}(f_3(a+c) + f_3(c)) \tag{9}$$

where the baseband-rate oscillating term $f_1(a\alpha(t)+c)$ in the control-data signal was averaged on T_{cont} (usually $T_{\text{cont}} \gg T_{\text{base}}$) supposing that 0 b and 1 b on the baseband signal are equiprobable. On the baseband signal amplitude, a worst-case

value was chosen for the control-channel induced-crosstalk term.

Using (8) and (10), Q_{base} and Q_{cont} can be expressed as functions of a, b, c and can, consequently, be optimized under given constraint. It is reasonable to set $Q_{\text{base}} = Q_{\text{cont}}$ to have the same BE probability on control-channel and baseband data. The optimization process should, consequently, look for the set of parameters a, b, c which give the maximum Q_{base} under the constraint $Q_{\text{base}} = Q_{\text{cont}}$. In other words, introducing $Q = \min(Q_{\text{base}}, Q_{\text{cont}})$, we want to find the maximum of $Q(a, b, c)$ as a function of a, b, c. In one of the following sections, experimental results will be compared to those obtained using this analytical formulation.

IV. Experimental Results and Comparison with Theory

A. Hybrid Link Demonstration

The experimental transmitter and receiver shown in Fig. 3 were constructed in order to verify the effect of operating parameters on system performance as predicted by the analytical model discussed in the previous section, and to compare the experimental eye diagrams with the results of the discrete-time simulation.

The baseband portion of the signal is a 2.5-Gb/s OOK pseudorandom bit stream (PRBS) with variable amplitude $\pm V_{\text{base}}/2$. This signal is generated using a BE-rate (BER) tester followed by a fifth-order Bessel low-pass filter with $f_{3\,\text{dB}} = 1.8$ GHz to reduce high-frequency components—a bias-tee was used to allow addition of a variable bias-voltage V_{bias}. The OSCM control channel is generated by upconverting a 100-Mb/s PRBS OOK control channel to a 5.5-GHz subcarrier using a synthesized signal generator and a microwave mixer. The extinction ratio between the 0 and 1 states that the mixer output was measured to be greater than 30 dB. The baseband and subcarrier signals are applied to independent arms of an $LiNbO_3$ MZ modulator, with a $V_\pi = 3.0$ V and a 3-dB modulation bandwidth equal to 6 GHz.

The MZ output power is split to the baseband/OSCM receivers using a 4:1 splitting ratio with the received optical powers measured to be $P_{\text{base}} = -10.4$ and $P_{\text{cont}} = -16.4$ dBm. The baseband signal is detected using a p-i-n FET photodiode, then filtered with a third-order low-pass filter with $f_{3\,\text{dB}} = 1.8$ GHz, and displayed on an oscilloscope to measure the Q values from the resulting eye diagram. The control-data signal is detected by following a photodiode with a traveling-wave amplifier and fifth-order bandpass filter with center frequency of 5.5 GHz and $f_{3\,\text{dB}} = 500$ MHz. The electronic subcarrier signal is further amplified and incoherently detected using a Schottky diode followed by a low-pass filter with corner frequency $f_{3\,\text{dB}} = 100$ MHz to recover the digital control data.

We measured the SNR values Q_{base} and Q_{cont} as a function of the modulator input voltages. In Fig. 4 we show the results as a function of $a = V_{\text{base}}/V_\pi$ and $b = V_{\text{cont}}/V_\pi$ for two different values of V_{cont} corresponding to measured values of $b = 0.08$ and $b = 0.06$. The b values take into account the 2.7-dB rolloff of the modulator at 5.5 GHz. The bias-voltage V_{bias} was set to obtain the best performances for each point. The baseband SNR is strongly dependent on a, while the dependence on b is negligible and is obscured by measurement errors. On the contrary, control-data performances are strongly affected by both a and b. Assuming we want the baseband and control-data error rates to be equal ($Q_{\text{base}} = Q_{\text{cont}}$), the choice $a = 0.45$, $b = 0.08$ leads to $Q_{\text{base}} = Q_{\text{cont}} \simeq 9.3$, a value giving a good system margin over the target $Q = 6$ corresponding to an error-probability $P_e \simeq 10^{-9}$.

The experimental results are compared to results obtained using the analytical formulation (shown in Fig. 4). The predicted and experimental results are qualitatively similar illustrating that optimal BER conditions can be achieved for the baseband and control channels. The difference between analytical and experimental results on control-data performance are due to several effects neglected in the analytical model including intersymbol interference, nonideal filtering, nonideal response of the Schottky diode, and the approximations we used to model the MZ modulator and the receiver noise.

The resulting experimental eye diagrams at the baseband and control-data receiver outputs are shown in Fig. 5. The eye closure is mainly due to receiver noise and partially to the interchannel interference between baseband and control channel, due to the nonlinearities at the transmitter.

An interesting parameter to consider is the effect of bias voltage on optimal operating points. This measure characterizes link robustness to modulator drift and variation and is demonstrated through a second set of measurements with fixed $a = 0.45$ and $b = 0.08$, and a varying input bias. The results are shown in Fig. 4, where Q_{base} and Q_{cont} are shown as a function of the parameter

$$\epsilon = \frac{V_{\text{bias}} - V_{\text{opt}}}{V_\pi} \tag{10}$$

where V_{opt} is the optimum bias voltage for this situation. We verified that V_{opt} is the biasing point which satisfies (5), and correspond to a situation in which the two baseband operating points V_0 and V_1 introduced in the previous section are symmetric to the MZ middle point $-V_\pi/4$.

Considering the strong dependence of Q_{cont} on ϵ, to ensure $Q_{\text{cont}} \geq 6$, the bias voltage should be kept close to V_{opt} with a $\epsilon = \pm 10\%$ accuracy, showing that the analysis developed in this paper could also be used to determine the acceptable tolerances on the bias-voltage fluctuation.

B. MMIC Experimental Results

Several MMIC components were fabricated for use in the OSCM link presented in the previous section, and were realized using the Triquint Semiconductor HA2 and QED/A GaAs Enhancement/Depletion MESFET processes.

A MMIC mixer designed for control-channel transmission has been realized and is shown in both MMIC and packaged form in Fig. 6. Dual-gate topology is employed for better isolation between the local oscillator (LO) and intermediate frequency (IF). The mixer was used in the transmitter part of the OSCM link and the upconverted-header data signal

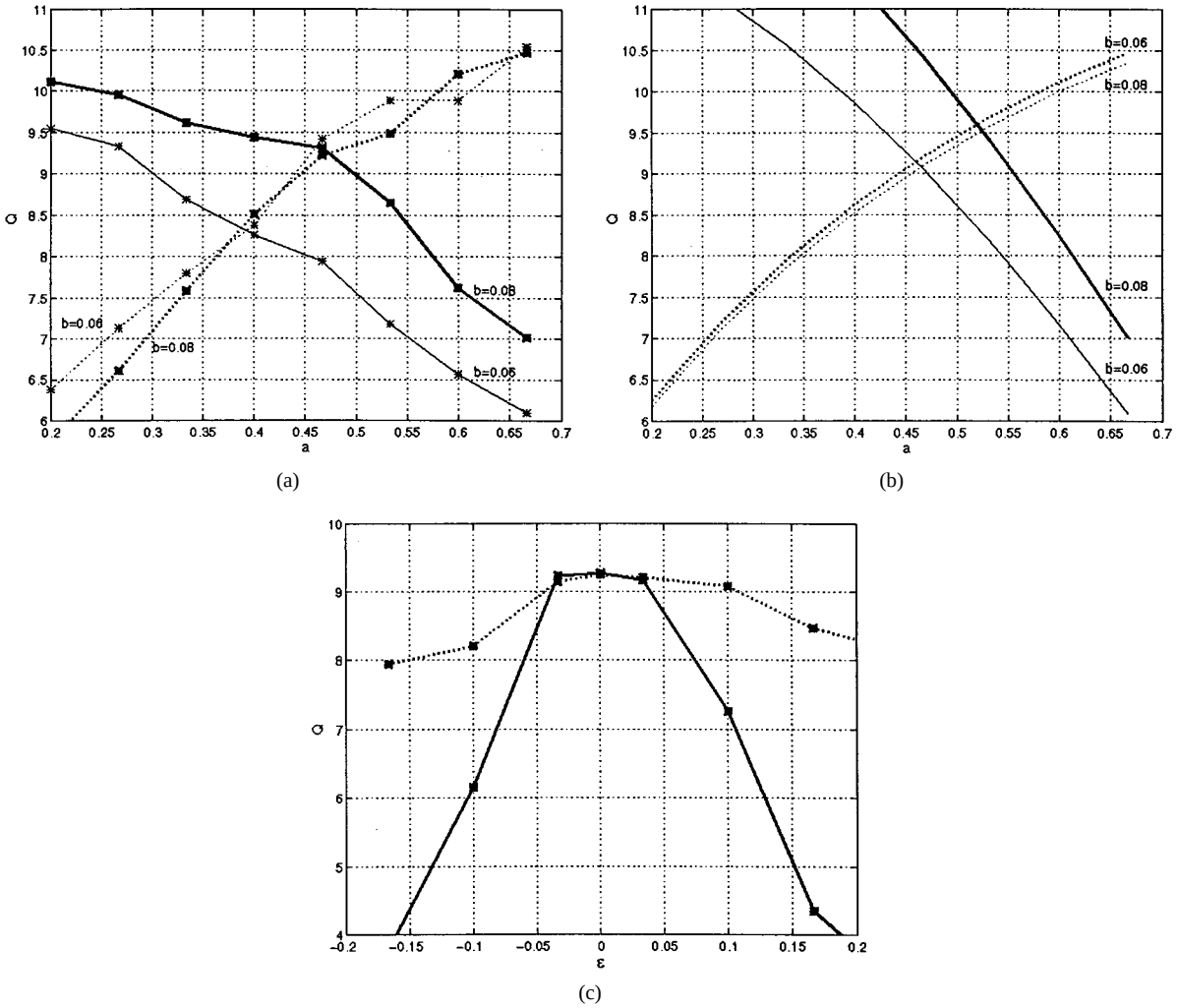

Fig. 4. (a) Experimental measurement of $Q_{\rm base}$ (dotted lines) and $Q_{\rm cont}$ (solid lines) as a function of a for two different values of b. (b) Comparison with analytical results. (c) Experimental measurement of $Q_{\rm base}$ (dotted lines) and $Q_{\rm cont}$ (solid lines) as a function of ϵ for $a = 0.475, b = 0.08$.

is shown in Fig. 7 together with the received eye diagram. The measured Q in this case was 9.35, a value comparable to the one obtained in the previous section with a discrete mixer. A MMIC mixer was used for envelope detection at the receiver, again achieving comparable results with the discrete component.

Oscillators for subcarrier signal generation have also been realized. Common-gate single-FET configuration is used for simplicity and compact design. These devices generate 2.5-, 3.5-, 4.5-, and 9-GHz carriers. One of these oscillators is shown in Fig. 8, together with its output spectrum. We are currently designing and processing more MMIC components to improve OSCM link performance.

V. Impact of MMIC Insertion

In this section, we investigate the potential enhancement obtained through the use of MMIC's in the baseband/OSCM link and show the discrete-time link simulation. The link simulation enables us to investigate the tradeoffs between complexity and performance improvement using MMIC technology for the photonic/microwave interfaces at the transmitter and receiver. MMIC insertion has the potential to impact performance through greater system margins, which can consequently be used to allow an increased control-channel bit-rate, a reduced splitting ratio for the control-channel receiver to the advantage of the baseband channel, and/or relaxed photonic components requirements. Moreover, MMIC realization has well-known advantages over discrete components in terms of size, interconnection losses, and ease of integration, particularly when used for very high baseband bit-rates (greater than 10 Gb/s) and high subcarrier frequencies (greater than 15 GHz).

We used the Series IV communications design suite from HP-EESOF to analyze the link architecture described in Fig. 1. The parameters were chosen to match those used in the experiment described in Section IV. We were able to use standard library building blocks for all the components (laser, fiber, filters, amplifiers, mixers, etc.) with the exception of the MZ external modulator, which was modeled as a user-defined block implementing (6), the photo-detector, whose noise is modeled with an ideal unity gain amplifier, and the Schottky diode, which was modeled as an ideal RF envelope detector.

The Series IV discrete-time test bench is used to process signals and noise together and generates time-domain output signals, which can then be post-processed to obtain eye diagrams, Q, and power spectra. Simulated eye diagrams are shown in Fig. 9. The evaluated Q is 7.7, which is slightly

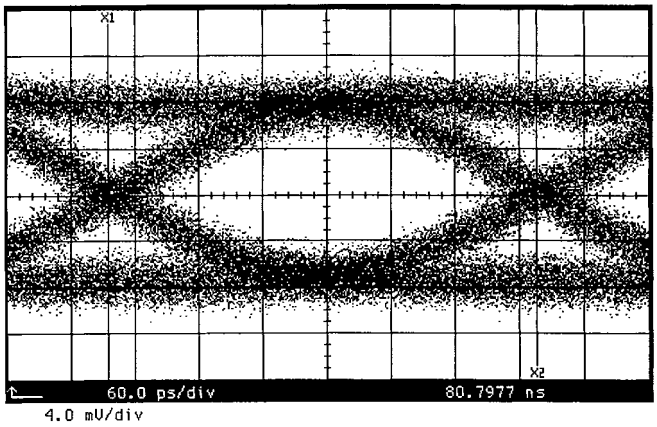

(a)

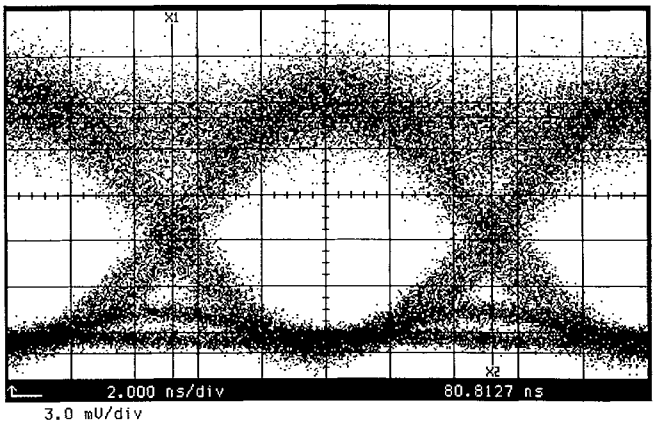

(b)

Fig. 5. Experimentally measured baseband (a) and control-channel (b) eye diagrams for $a = 0.45$, $b = 0.08$.

lower than experimental result. This discrepancy is primarily due to differences in the turn-on characteristics of the Schottky detector and in modeling of the MZ modulator. The obtained eye closure is due to noise and nonlinear crosstalk introduced between the baseband and subcarrier signals.

Finally, we have used the simulator to study the impact of MMIC insertion on link performance. We have designed several MMIC-chip sets which are currently being processed. We predict an improved link performance based upon the following simulated MMIC characteristics. First, the LO feedthrough of the control-channel mixer is improved by 5 dB. Second, the noise figure of the broad-band amplifier following the photodetector is reduced from 8 dB, as in the discrete amplifier used in the experiment, to 2 dB.

In Fig. 9, we show the eye diagram of the simulated control channel. The simulated Q is 8.3, which has been improved with respect to the link simulation reported in previous paragraph. This example shows how system margins can be increased by MMIC insertion and how the potential gains can be verified by simulation.

VI. Conclusion and Future Work

We have reported new results for the design, analysis, simulation, and experimental demonstration of a high-performance fiber transmission link which supports parallel transmission

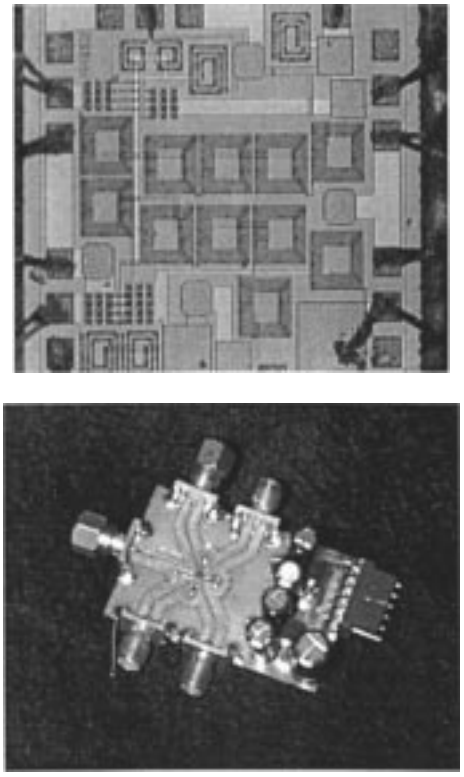

Fig. 6. Photographs of MMIC mixer in chip and packaged forms.

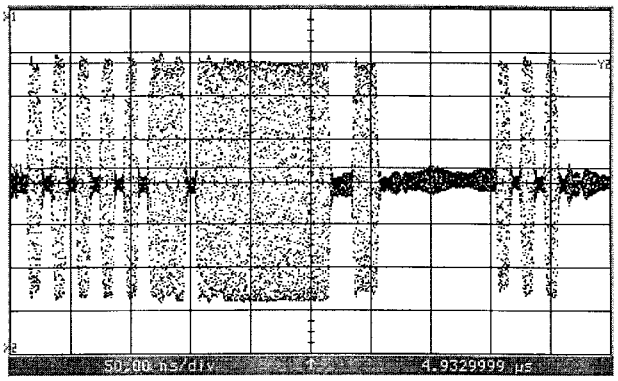

(a)

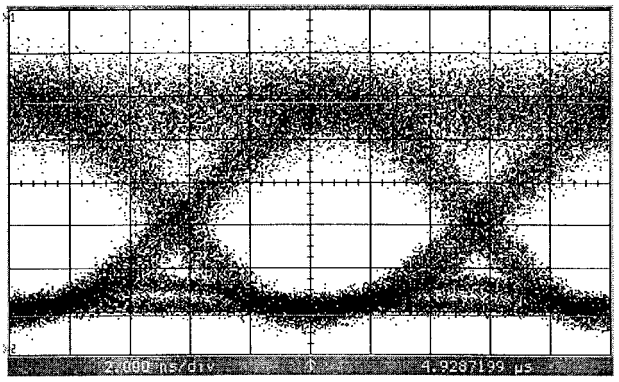

(b)

Fig. 7. (a) Subcarrier encoded control-channel signal at the output of the transmitter MMIC mixer and (b) eye diagram of the detected signal.

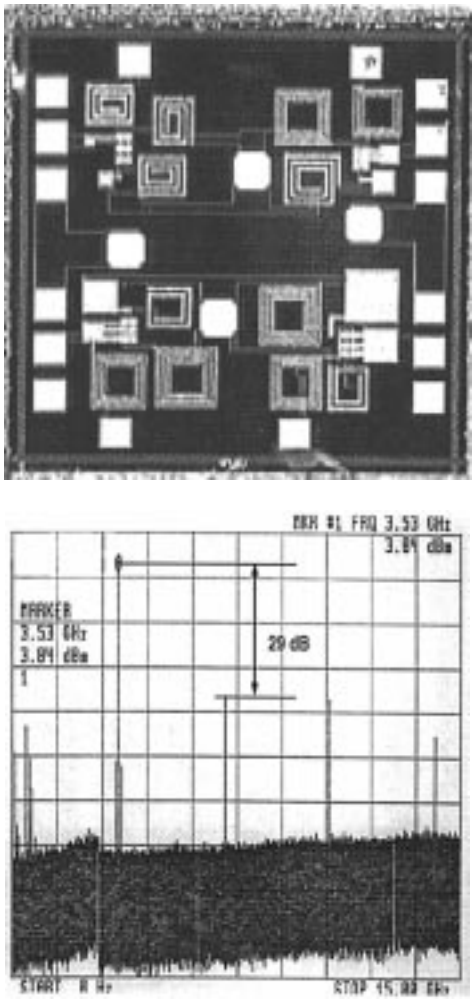

Fig. 8. 3.5-GHz MMIC oscillator. Photograph of the chip and measured output power spectrum.

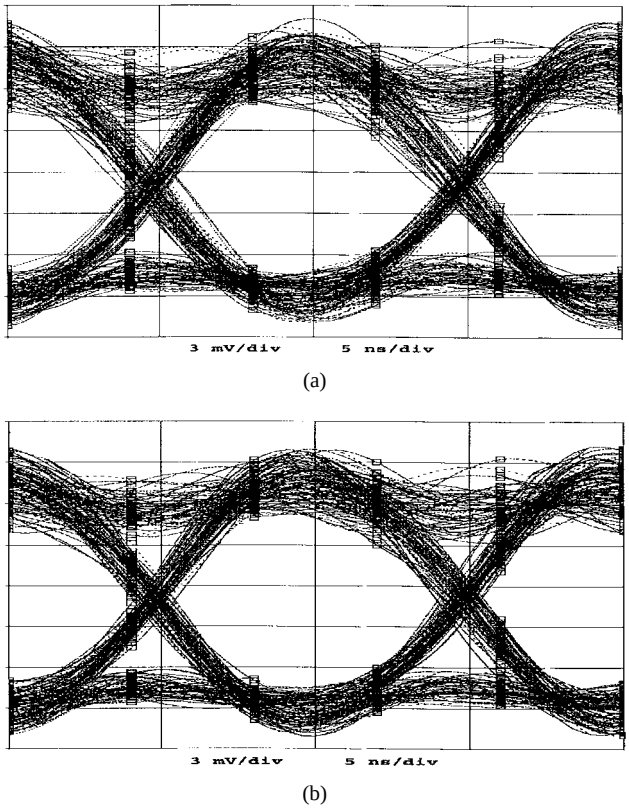

Fig. 9. (a) Eye diagram of simulated recovered subcarrier control channel. (b) Improvement due to MMIC insertion.

of baseband data and out-of-band control data using OSCM. Key features of the architecture include the use of a novel differential optoelectronic combiner in the baseband/OSCM transmitter and a direct-detection microwave subcarrier receiver. These features greatly simplify the overall transmitter/receiver implementation and make MMIC implementation more practical. In order to understand the link performance and impact of MMIC insertion, a new parameter optimization model for the transmitter was developed. Once the parameters were optimized, a time-domain simulation provided detailed information about performance of the baseband and control-data channels based on detailed knowledge of the device parameters, operating characteristics, and noise parameters. We compared the discrete implementation of the link with MMIC implementation of photonic/microwave interfaces in the transmitter and receiver. This comparison was performed at optimal operating points determined by our analytical model. Both the analytical model and discrete-time simulation utilized parameters obtained from an experimental demonstration. The theoretical and simulation results were then compared to experimental results and found to be in good agreement. Simulation of the link with MMIC insertion also showed an improvement in performance of the SNR of the received eye diagrams. Finally, we presented results of MMIC realization of oscillators and upconverters for use in the described link architecture.

Ongoing and future efforts will focus on further developing a methodology and procedure for inter-relating the architecture, optimization, simulation, experimentation, and MMIC integration. Specific areas pertaining to parameter optimization include evaluation of different modulator transfer functions, different modulation formats, and the impact of optical amplification. With respect to simulation efforts, more complex MZ electro-optic modulator and nonlinear electrical components models will be inserted. Monolithic integration of more system components onto a single chip will be performed in addition to studying the upper boundaries on subcarrier frequencies using MMIC technology.

REFERENCES

[1] R. Olshansky, V. A. Lanzisera, and P. M. Hill, "Subcarrier multiplexed lightwave systems for broad-band distribution," *J. Lightwave Technol.*, vol. 7, pp. 1329–1342, Sept. 1989.

[2] T. E. Darcie, "Subcarrier multiplexing for lightwave multiple-access networks," in *Opt. Fiber Commun. Conf. and Sixth Int. Conf. Integrated Optics and Opt. Fiber Commun.—Tech. Dig.*, Reno, NV, Feb. 1987, pp. 31–32.

[3] S. F. Su and R. Olshansky, "Performance of WDMA networks with baseband data packets and subcarrier multiplexed control channels," *IEEE Photon. Technol. Lett.*, vol. 5, pp. 236–239, Feb. 1993.

[4] T. H. Wood, R. D. Feldman, and R. F. Austin, "Demonstration of a cost-effective, broad-band passive optical network system," *IEEE Photon. Technol. Lett.*, vol. 6, pp. 575–578, Apr. 1994.

[5] K.-I. Kitayama, "Subcarrier multiplexing based signaling and access control in optical FDM networks," presented at the *Proc. IEEE Global Telecommun. Conf.*, pt. 3, Singapore, May 1995.

[6] M. W. Maeda, A. E. Willner, J. R. I. Wullert, J. Patel, and M. Allersma, "Wavelength-division multiple-access network based on centralized common-wavelength control," *IEEE Photon. Technol. Lett.*, vol. 5, pp. 83–85, Jan. 1993.
[7] N. J. Frigo *et al.*, "Wavelength-division multiplexed passive optical network with cost-shared components," *IEEE Photon. Technol. Lett.*, vol. 6, pp. 1365–1367, Nov. 1994.
[8] A. Budman, E. Eichen, J. Schlafer, R. Olshansky, and F. McAleavey, "Multigigabit optical packet switch for self-routing networks with subcarrier addressing," in *Conf. Opt. Fibers Commun.*, San Jose, CA, Feb. 1992, pp. 90–91.
[9] P. Poggiolini and S. Benedetto, "Theory of subcarrier encoding of packet headers in quasi-all-optical networks," *J. Lightwave Technol.*, vol. 12, pp. 1869–1881, June 1994.
[10] C.-L. Lu, T. K. Fong, R. T. Hofmeister, P. Poggiolini, and L. G. Kazovsky, "CORD—A WDM optical network: Design and experiment of fast data synchronization by pilot-tone transport," *IEEE Photon. Technol. Lett.*, vol. 8, pp. 1070–1072, Aug. 1996.
[11] M. Shell, M. D. Vaughn, A. Wang, D. J. Blumenthal, P. J. Rigole, and S. Nillson, "Experimental demonstration of an all-optical routing node for multihop wavelength routed networks," *IEEE Photon. Technol. Lett.*, vol. 8, pp. 1391–1393, Oct. 1996.
[12] J. Conradi, B. Davies, M. Sieben, D. Dodds, and S. Waklin, "Optical single sideband transmission for dispersion avoidance and electrical dispersion compensation in microwave subcarrier and baseband digital systems," presented at the *OFC'97*, Dallas, TX, Feb. 1997.
[13] M. T. C. Silva, M. A. G. Martinez, and P. R. Herczfeld, "MQW optical modulators for InP based MMIC/photonics integrated circuits," in *IEEE MTT-S Int. Microwave Symp. Dig.*, Atlanta, GA, June 1993, pp. 229–232.
[14] K. E. Alameh and R. A. Minasian, "Tuned optical receivers for microwave subcarrier multiplexed lightwave systems," *IEEE Trans. Microwave Theory Tech.*, vol. 38, pp. 546–551, May 1990.
[15] D. J. Blumenthal, M. Shell, Q. Gao, M. Vaughn, A. Wang, P. Rigole, and S. Nilsson, "Experimental demonstration of an all-optical multihop routing node for wavelength routed networks," presented at the *Conf. Opt. Fibers Commun.*, San Jose, CA, 1996.
[16] E. Park and A. E. Willner, "Network demonstration of self-routing wavelength packets using an all-optical wavelength shifter and QPSK subcarrier routing control," presented at the *Conf. Opt. Fibers Commun.*, San Jose, CA, 1996.
[17] P. Poggiolini and S. Benedetto, "Performance analysis of multiple subcarrier encoding of packet headers in quasi-all-optical WDM networks," *IEEE Photon. Technol. Lett.*, vol. 6, pp. 112–114, Jan. 1994.
[18] T. E. Darcie, M. E. Dixon, B. L. Kasper, and C. A. Burrus, "Lightwave system using microwave subcarrier multiplexing," *Electron. Lett.*, vol. 22, pp. 774–775, July 1986.

Daniel J. Blumenthal (S'91–M'93) received the B.S.E.E. degree from the University of Rochester, Rochester, NY, in 1981, the M.S.E.E. degree from Columbia University, New York, NY, in 1988, and the Ph.D. degree from the University of Colorado at Boulder, in 1993.

In 1981, he joined StorageTek of Louisville, CO, where he was engaged in research and development in optical data storage systems. In 1986, he worked at Columbia University as a Research Engineer in the areas of photonic switching systems and ultrafast all-optical networks and signal processing. In 1990, he worked as a Graduate Research Assistant on multiwavelength photonic switched interconnects for distributed computing applications. He is currently an Assistant Professor in the School of Electrical and Computer Engineering, Georgia Institute of Technology, Atlanta, and heads the Optical Communications and Photonic Networks (OCPN) Research Networks. His current research areas are in optical communications, WDM, photonic-switched and all-optical networking, wavelength conversion in semiconductor devices, and optical information processing. He has authored or co-authored over 30 papers in these and related areas.

Dr. Blumenthal is a member of the IEEE Optical Society of America, and the Lasers and Electrooptic Society. He is currently an associate editor for the IEEE PHOTONICS TECHNOLOGY LETTERS AND IEEE TRANSACTIONS ON COMMUNICATIONS. He is also chair of the LEOS Atlanta Chapter and serves on the Program Committee for the 1997 and 1998 Conference on Optical Fiber Communications (OFC). In 1994, he was recipient of an NSF Young Investigator Award, and in 1997, he received an Office of Naval Research Young Investigator Award.

Joy Laskar (S'84–M'85) received the B.S. degree in computer engineering (highest honors) from Clemson University, Clemson, SC, in 1985, and the M.S. and the Ph.D. degrees in electrical engineering from the University of Illinois at Urbana-Champaign, in 1989 and 1991, respectively.

In 1985, he was employed at IBM's Thomas J. Watson Research Center, where he studied hot-electron effects in sub-micron CMOS technology. From 1991 to 1992, he served as Visiting Assistant Professor at the University of Illinois. From 1992 to 1994, he served as Assistant Professor at the University of Hawaii at Manoa. He is responsible for the establishment of the Microwave Applications Group. Since 1991, his research on high frequency device design and characterization has been supported by ARPA, NASA, and several industrial laboratories including Cascade Microtech, Hewlett-Packard, Lockheed-Martin, Panda Technologies, Packaging Research Center, NEC, Texas Instruments, Triquint Semiconductor and TRW. His research interests include millimeter-wave devices and circuits and their applications. He has primarily been concerned with the development of cryogenic, on-wafer characterization techniques through 110 GHz with applications to monolithic microwave integrated circuits (MMIC's), with ongoing research interests including development of ultra-low noise amplifiers based upon InP HEMT technology with applications to both ground- and space-based MMIC receiver components, development of on-wafer characterization techniques with applications to MMIC's and high-speed packages, study of advanced III–V transistor structures for ultra-high speed operation, application of MMIC design, and characterization techniques to optoelectronic integrated circuits.

Dr. Laskar is a co-organizer for the Advanced Heterostructure Workshop and serves on the IEEE Microwave Theory and Techniques Symposia Technical Program Committee. In 1995, he received the Army Research Office Young Investigator Award, and the NSF Career Award in 1996.

Roberto Gaudino received the Laurea degree in ingegneria elettronica (*summa cum laude*) from Politecnico di Torino, Torino, Italy, in 1993, and is currently working toward the Ph.D. degree in electrical engineering (optical communications).

He is currently a Visiting Scholar at the Georgia Institute of Technology, Atlanta, where he works on topics related to optical networks in the Optical Communication and Photonic Network (OCPN) Group. His main research interests are focused on optical communications in general and, in particular, on polarization modulation.

Mr. Gaudino's graduation thesis on polarization modulation was granted an award by Telecom Italia and by Fondazione Ugo Bordoni (Rome, Italy).

Sangwoo Han (S'94–M'96) received the B.S. degree in electrical engineering from Carnegie-Mellon University, Pittsburgh, PA, in 1992, and the M.S. degree in electrical engineering from University of Pennsylvania, Philadelphia, in 1994. He is currently working toward the Ph.D. degree at the Georgia Institute of Technology, Atlanta, where he works as a Research Assistant in the Microwave Applications Group.

His research interest include system simulation and optimization techniques, and design and testing of MMIC circuits for wireless and telecommunication applications, and on wafer noise characterization of high-speed devices.

Michael D. Shell received the B.E.E. and M.S.E.E. degrees from the Georgia Institute of Technology, Atlanta, in 1991 and 1993, respectively, and is currently working toward the Ph.D. degree.

He has worked on the development of several WDM all-optical network subsystems including packet-switching nodes, high-speed tunable lasers, and a multiwavelength-laser array transmitter.

Mark D. Vaughn received the B.A. degree in physics from Alfred University, Alfred, NY, in 1991, and the M.S. degree in optics from the Institute of Optics, University of Rochester, Rochester, NY, in 1993. He is currently working toward the Ph.D. degree in electrical engineering at the Optical Communications and Photonic Networks (OCPN) Laboratory, Georgia Institute of Technology, Atlanta.

His research focus is on optical subcarrier multiplexed signal processing. Since 1988, he has been employed by Corning Inc., Corning, NY, working in the area of optoelectronics research.